2013

THE HOLOGRAPHIC DETECTOR FOR CLOUDS FROM TRL 5 TO TRL 8

Matthew Jacob Beals
Michigan Technological University

THE HOLOGRAPHIC DETECTOR FOR CLOUDS FROM TRL 5 TO TRL 8

By
Matthew Jacob Beals

A REPORT
Submitted in partial fulfillment of the requirements for the degree of
MASTER OF SCIENCE
In Electrical Engineering

MICHIGAN TECHNOLOGICAL UNIVERSITY
2013

This report has been approved in partial fulfillment of the requirements for the Degree of MASTER OF SCIENCE in Electrical Engineering.

Department of Electrical and Computer Engineering

Report Co-Advisor *Dr. Michael Roggemann*

Report Co-Advisor *Dr. Raymond Shaw*

Committee Member: *Dr. Timothy Schulz*

Department Chair: *Dr. Daniel Fuhrmann*

Contents

List of Figures

List of Tables

Acknowledgments

I would like to thank all of the staff at the Research Aviation Facility of the National Center for Atmospheric Research and the University of Wyoming flight center. Without their hard work and dedication, development and testing of the Holodec instrument would not have been possible. I would specifically like to thank the engineers and technicians for their assistance, insight and patience during the tribulations encountered during field testing, as well as their guidance during the redesign. Their help and support was instrumental in advancing the instrument to the level it is today.

In addition, I would like to thank Dr Jacob Fugal for his role in the initial development of the Holodec instrument and his continuing involvement with the development of the processing code. His input and assistance was crucial to the success of this project as well as my continuing research.

I would also like to thank my advisors, Dr Raymond Shaw, Dr Michael Roggemann and Dr. Timothy Schulz for their continued support, assistance and guidance in this endeavor.

This research was supported by the Office of Biological and Environmental Research of the U.S. Department of Energy under grant number 6021382 as part of the Atmospheric Radiation Measurement Climate Research Facility, by the U.S. National Science Foundation (AGS-1026123) and by a NASA Earth Systems Science Fellowship (2011-2013).

Abstract

Clouds are one of the most influential elements of weather on the earth system, yet they are also one of the least understood. Understanding their composition and behavior at small scales is critical to understanding and predicting larger scale feedbacks. Currently, the best method to study clouds on the microscale is through airborne *in situ* measurements using optical instruments capable of resolving clouds on the individual particle level. However, current instruments are unable to sufficiently resolve the scales important to cloud evolution and behavior.

The Holodec is a new generation of optical cloud instrument which uses digital in-line holography to overcome many of the limitations of conventional instruments. However, its performance and reliability was limited due to several deficiencies in its original design. These deficiencies were addressed and corrected to advance the instrument from the prototype stage to an operational instrument. In addition, the processing software used to reconstruct and analyze digitally recorded holograms was improved upon to increase robustness and ease of use.

1 Introduction

1.1 Scientific Motivation

Clouds play a critical role in the hydrological processes and radiative balances which make life on the planet earth possible. For instance, cirrus clouds have a very large impact on the earth's radiative budget [19] [13] and the hydrological cycle [20]. These effects (which can impact very large areas) are mostly governed by small scale properties of the cloud, such as ice water content, particle size, ice particle shape and particle number density (concentration) [14].

Quantifying the cloud particle size distribution requires measuring at least three parameters as accurately as possible: the shape, size, and phase of individual particles; the total number of each type of particle; and the total volume of cloud sampled. Currently, these measurements are made by optical instruments that are designed to sample and measure a single particle at a time. This 'single particle at a time' strategy suffers from several serious deficiencies. These include, coincident particles in the sample volume being counted as a single large particle (leading to anomalously high counts in certain size bins) and the sample volume size being a function of particle size or otherwise poorly characterized.

This sampling strategy also requires samples to be integrated over tens or hundreds of meters to form a statistically significant volume. This places a fundamental limit on the spatial resolution of computed parameters (such as size distributions, number densities and ice - water fractions) of roughly 100m (1s at $100\,m/s$) [11]. However, the scales that are important to cloud development and evolution (e.g. diffusion, evaporation and phase relaxation length scales) are typically on the order of centimeters. This scale of interest is well below what is possible to measure with traditional instruments.

Mixed phase clouds also present a special challenge to the field of remote sensing. Their composition is extremely important, as it can greatly influence satellite retrievals [16] and radiation transfer calculations [15] but *in-situ* measurements have been greatly limited by a lack of aircraft instrumentation that can discriminate between the ice and liquid phases over a wide range of sizes [11]. Korolev *et al* [11] present instruments capable of measuring total water and liquid water contents (and thus ice/water ratios), but parameters critical to understanding the cloud's radiative properties (such as particle size and particle number density) can only be reliably measured with optical probes. However, the same sampling problem still applies, and the mixed phase environment introduces a number of new problems, including contamination by ice crystal shattering [3] [10] [12].

Many of these limitations can be overcome by abandoning the 'single particle at a time' sampling strategy for a more generalized 'volume at once' approach. This is realized through the use of holography. In-line holography is a technique that allows for an entire population of particles to be imaged at once. This preserves their three dimensional position in the volume as well as their two dimensional outline.

Holography has a number of advantages over traditional instruments. Particle detectability (to within resolution limits) is uniform for all particle sizes, making the sample volume size well characterized. In addition, the technique allows for large sample volume sizes and a large range of detectable sizes. This allows each hologram to potentially stand as an individual, statistically significant volume while also allowing it to measure a much broader range of particle sizes than existing instruments. The three dimensional position and particle shape preserved in the hologram can also be used to study the spatial correlations of particles and ice in the presence of liquid water down to very small scales. This represents an ability not currently possible with existing instruments.

The application of in-line holography to airborne *in situ* cloud measurements was first attempted by Brown in the late 1980's[2] with an instrument that consisted of a pulsed laser illuminating large format photographic film. While successful, this instrument was greatly limited by the reconstruction process which could take a skilled operator several hours to catalog enough particles to form a single statistically significant size distribution.

The limitations imposed by film-based recording and reconstruction methods were finally overcome with the advent of digital imaging technology. This technology was applied by Fugal to create the first generation HOLOgraphic DEtector for Clouds (Holodec) instrument[5]. Successful flight testing of this instrument[4] prompted the development of the second generation instrument on which this report is based.

1.2 Technology Readiness Level

My work with the Holodec II (referred to from here as just the Holodec) began in 2009, just prior to final construction and testing. At this point in the instrument's development cycle, the systems required for hologram formation and recording were in a mature state, but supporting systems (control and environmental conditioning) were not. These subsystems were functional, but were not optimized or well integrated. This resulted in various performance deficiencies that I worked to address. Specifics are detailed in section 3.

The state of an instrument in the development cycle can be defined by a "Technology Readiness Level" or TRL. The work I performed was funded by the Department of Energy (DOE) under an instrument improvement and hardening grant (number: 6021382). Portions of this report have been adapted from the final report submitted outlining the work performed[17]. Therefore, the TRL values cited in this work will follow the DOE scale, which is outlined in table 1.1.

At the beginning of the work, the Holodec was classified at TRL 5. While the instrument was operating in the field (which would classify it as TRL 6 or above), it was felt that the instrument did not represent a "major step up" in readiness from the "breadboard technology" of TRL 5. This was due to several observed limitations in the instrument design that resulted in less than desirable performance and robustness, as well as the inability to properly perform in all expected environmental conditions.

The goal of the work presented in this report is to increase the instrument to at least TRL 8, which corresponds to "Actual technology completed and qualified through test and demonstration". This represents bringing the instrument out of the prototype stage and to a fully operational level, as well as maturing the onboard systems to better handle the harsh environments experienced during high altitude flight.

Table 1.1: Description of Department of Energy (DOE) Technology Readiness Levels (TRL) [1]

TRL 1	Scientific research begins translation to applied R&D - Lowest level of technology readiness. Scientific research begins to be translated into applied research and development. Examples might include paper studies of a technology's basic properties.
TRL 2	Invention begins - Once basic principles are observed, practical applications can be invented. Applications are speculative and there may be no proof or detailed analysis to support the assumptions. Examples are limited to analytic studies.
TRL 3	Active R&D is initiated - Active research and development is initiated. This includes analytical studies and laboratory studies to physically validate analytical predictions of separate elements of the technology. Examples include components that are not yet integrated or representative.
TRL 4	Basic technological components are integrated - Basic technological components are integrated to establish that the pieces will work together.
TRL 5	Fidelity of breadboard technology improves significantly - The basic technological components are integrated with reasonably realistic supporting elements so it can be tested in a simulated environment. Examples include "high fidelity" laboratory integration of components.
TRL 6	Model/prototype is tested in relevant environment - Representative model or prototype system, which is well beyond that of TRL 5, is tested in a relevant environment. Represents a major step up in a technology's demonstrated readiness. Examples include testing a prototype in a high-fidelity laboratory environment or in simulated operational environment.
TRL 7	Prototype near or at planned operational system - Represents a major step up from TRL 6, requiring demonstration of an actual system prototype in an operational environment.
TRL 8	Technology is proven to work - Actual technology completed and qualified through test and demonstration.
TRL 9	Actual application of technology is in its final form - Technology proven through successful operations.

2 Digital In-line Holography and the Holodec

2.1 The Holodec

The Holographic Detector for Clouds (Holodec), (Figure 2.1) is a holographic instrument capable of imaging a $20\,cm^3$ volume of cloud air at a rate of 3.3 Hz. The instrument has a theoretical lower particle resolution of approximately 6 μm and an upper limit of several mm [18] allowing for ice detection down to approximately $30\,\mu m$. The measurement is inherently three-dimensional such that each particle in the sample volume is counted and artifacts resulting from shattered ice crystals can be identified. The sample volume of each hologram is also precisely known, and in fact, can be adjusted as part of the digital reconstruction process [7].

The sample volume size of the Holodec is large enough that each hologram represents a statistically significant population for typical cloud droplet sizes and concentrations. By eliminating the necessity to combine multiple volumes to obtain accurate size distributions and number densities, this allows each hologram to stand alone as a discrete measurement. This combined with the 3-D particle position and particle phase information allows for detailed analysis of the cloud's spatial structure at scales critical to cloud microphysical processes.

(a) NCAR C-130

(b) U. Wyoming King Air

Figure 2.1: Holodec II mounted on the (a) NCAR C-130 and (b) University of Wyoming King Air . Also shown are two versions of the 2-DC (bottom and middle in a) and the FSSP (left in b).

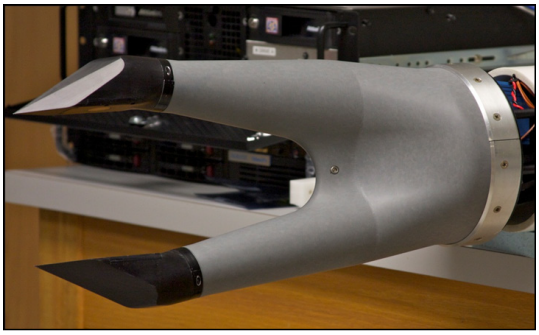

(a) Front half of Holodec instrument showing optical tips and flow shroud.

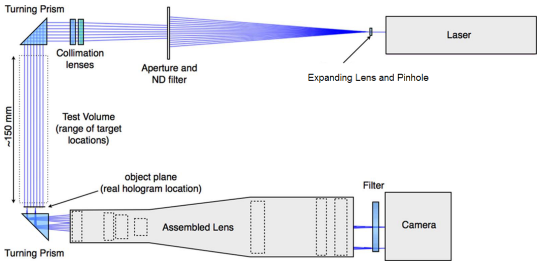

(b) Internal layout of instrument showing optical path

Figure 2.2: Layout of Holodec II instrument. Camera and laser are both housed in the body of the instrument just behind the gray flow shroud in (a), with main beam path (including optics assembly) located in the instrument's arms. Collimation optics and turning prisms are housed in black optical tips which define the location and width of the sample volume. Tips are shaped to reduce contamination of sample volume due to airflow deformation and ice crystal shattering[9].

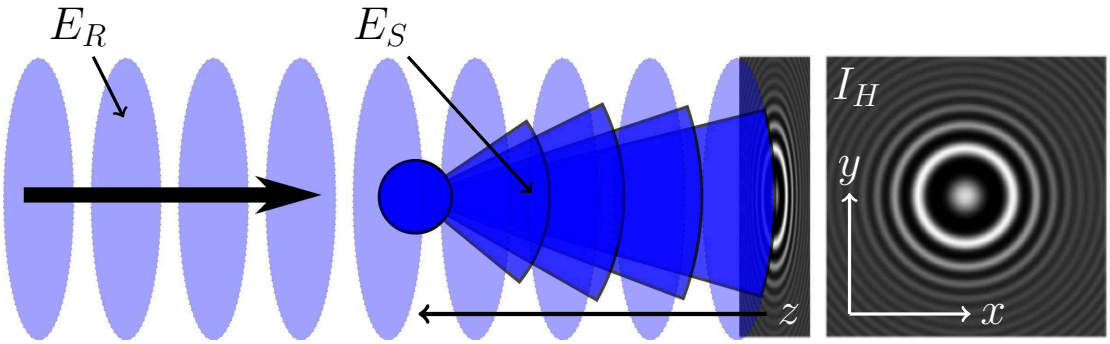

Figure 2.3: Illustration of the recording process for in-line holography. Light forward scattered by particles illuminated by the main beam interferes with the main beam itself, producing the interference pattern that forms the hologram.

2.2 Hologram Formation

The Holodec makes use of the in-line geometry to form holograms. In this geometry (figure 2.3), both the object and reference beams (of typical off-axis geometry) are combined into a single illuminating beam (E_R). When a particle (or dilute suspension of particles) is illuminated, the resulting scattered light (E_S) interferes with the illuminating beam. An interference pattern is formed, which can be recorded by a digital detector. This is the arrangement used in the Holodec and is illustrated in figure 2.2. The source of illumination is a filtered, expanded and collimated laser beam, which illuminates an interline CCD through a specially designed, 2.5× magnification, a-focal lens system.

The field at the detector (E_H) can be interpreted as the modulus squared of the superposition of the two waves: $I_H = |E_H|^2 = |E_R + E_S|^2$. Expansion of this expression results in

$$I_H = E_H E_H^* = \underbrace{E_R E_R^*}_{\text{background}} + \underbrace{E_R E_S^*}_{\text{real image}} + \underbrace{E_S E_R^*}_{\text{virtual image}} + E_S E_S^* \tag{2.1}$$

For the application of sensing cloud particles in the range of hundreds of micrometers, $E_S << E_R$, causing the final term to become negligible. The background (first) term represents the contribution to the hologram of the reference beam itself. This term can be mostly negated through the process of background division, which involves dividing the hologram by a 'typical' background formed by taking the pixel-wise median of several surrounding holograms. This method reduces the contrast of features that are shared between holograms, helping to smooth low frequency intensity fluctuations in the laser beam profile as well as reduce the visibility of particles adhering to the optics (which are considered con-

taminants)[7]. The second two terms (the 'real image' and 'virtual image') contain the information related to the sampled particles' three dimensional position and two dimensional shape. Due to the in-line geometry used, the real and virtual images form in coincident locations in the (x, y) plane with equal but opposite z (see figure 2.3 for geometry).

2.3 Reconstruction Method

In the in-line geometry, each particle in the field can be approximated as an ideal obscuration located at some discrete distance (z) from the recording plane. By assuming that the effects of secondary scattering are negligible (valid for tenuous suspensions), this hologram can be approximated as the superposition of the collection of interference patterns created by each individual aperture function. For a film hologram, illuminating the holographic plate with a copy of the original reference wave would produce images of the original obscurations (particles) where they occurred in the original test volume. For a digital hologram, we use the digital analog to this process.

If we consider an arbitrary, two dimensional field $g(x, y)$, the Fourier transform of this field can be seen to form a linear combination of phasors of phase $\phi = 2\pi(f_x x + f_y y)$.

$$FT\{g(x,y)\} = A(f_x, f_y) = \iint_{-\infty}^{\infty} g(x,y) e^{j2\pi(f_x x + f_y y)} dx dy \tag{2.2}$$

With some math (see chapter 3 of Goodman for details[8]), it can be shown that these phasors can be associated with individual spatial frequency pairs (f_x, f_y) through the angular spectrum.

Through a process involving solving the Rayleigh Sommerfield and Helmholtz equations (see chapter 3 in Goodman[8]), an exact solution can be found that predicts the phase shift of individual phasors in the angular spectrum due to propagating the field a distance z parallel to the optical axis. This function is known as the transfer function of free space propagation (H) and has form:

$$H(f_x, f_y, z) = \exp\left(j\tfrac{2\pi}{\lambda} z \sqrt{1 - \lambda^2(f_x^2 + f_y^2)}\ \right). \tag{2.3}$$

Multiplying the angular spectrum of the hologram by $H(z')$ results in the angular

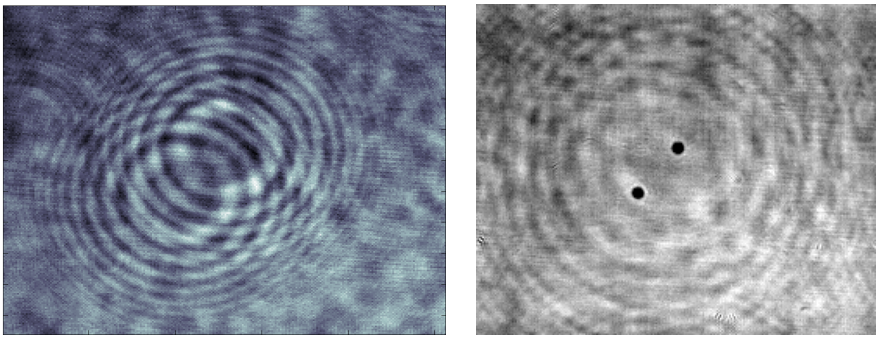

(a) Hologram **(b)** Reconstructed field

Figure 2.4: Example of an in-line hologram (a) and reconstructed slice (b) showing the particles in focus.

spectrum in the (x, y) plane of the field at a distance z' from the hologram. The aperture function at z' that would result in the observed hologram can then be recovered through the inverse Fourier transform of this product.

$$g(x, y, z') = FT^{-1}\left\{A_H H(z)\right\} = FT^{-1}\left\{A_H \exp\left(j\tfrac{2\pi}{\lambda} z\sqrt{1-\lambda^2(f_x^2+f_y^2)}\;\right)\right\}, \tag{2.4}$$

where A_H denotes the angular spectrum of the hologram field. If a particle happened to exist at z', the recovered field ($g(x, y, z')$) will contain that particle's geometric cross section as well as interference fringes from all other particles that remain out of focus. An example reconstruction is shown in figure 2.4. The left image (a) is of the raw hologram and the right (b) is of a reconstructed slice where the two particles are in focus.

It is important to recognize that the recorded hologram (and therefore the reconstructed field) is band limited by the recording system with cutoff frequency (and therefore diffraction limited resolution) decreasing with increasing distance from the detector. The in-focus image (which should closely approximate an ideal rectangle function in cross section) of particles that happen to lie outside of this diffraction limit will begin to blur and lose sharpness as higher frequencies are truncated. Since detection and sizing rely on thresholds and pixel counting, this variable resolution limit can cause small particles to be sized artificially small (or be completely missed) with increasing distance from the detector. This is compensated for by limiting the bandwidth of all reconstruction distances to the bandwidth of the farthest through the application of a super-Gaussian low pass filter[7].

2.4 Particle Identification

The reconstruction process produces a single 'slice' of the complex field corresponding to the field along a plane lying parallel to the hologram plane. Both the amplitude and phase information contained within this field can be used in the process of particle identification and classification.

As discussed previously, the reconstructed image is an aperture function. Therefore, when the reconstructed image is in-focus, the pixel values corresponding to the particle (in the amplitude image) should be equal to zero. While this is not entirely true, in practice the values are still observed to drop significantly. This is shown more clearly in figure 2.5 which shows how values of both amplitude and phase vary with reconstruction depth for a fixed (x, y) position aligned with the center of one of the particles shown in figure 2.4b. The point at which the amplitude trace (blue) is at a minimum corresponds to the in-focus reconstruction depth.

Because of the sharp contrast between the pixels that represent the particle and the background, these pixels can be identified through the use of a simple threshold. An example of such a threshold is shown in figure 2.5 as the blue horizontal line. This threshold is chosen to be several standard deviations above the noise floor to maximize the recovered signal while minimizing the amount of noise (leading to false alarms). This forms the basis for the reconstruction technique: the hologram is reconstructed slice-by-slice with a uniform spacing in z (dz = constant). All 'qualified' (based on threshold) pixel values and their locations are then extracted for further processing.

The blue shaded region in 2.5 illustrates the depth through which 'qualified' pixels would be retrieved for the example particle during this iterative reconstruction

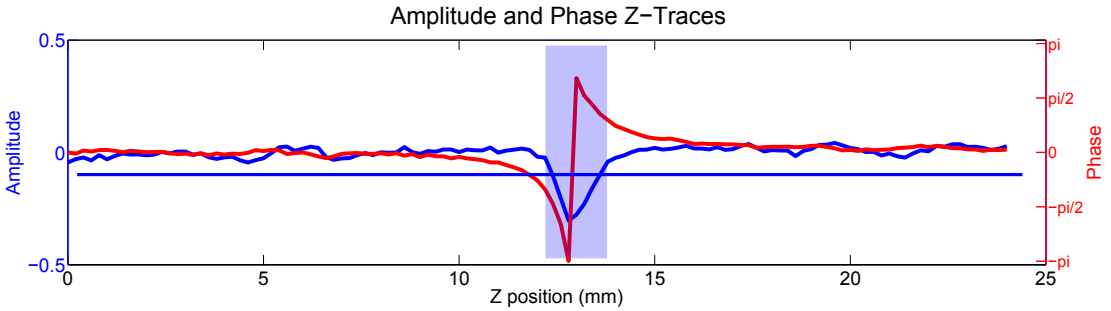

Figure 2.5: Linear profile (along z) of amplitude (blue) and phase (red) taken through center of a particle. Blue horizontal line indicates amplitude threshold used to classify pixels. Shaded blue region illustrates range of z values flagged by threshold.)

process. This apparent exaggeration of the depth of the particle is a realization of the depth of focus problem. This results in particles appearing to be in focus for a range of z values that scales as d^2/λ. While this effect does reduce the precision of estimates of the in-focus depth, it does allow the reconstruction process to be performed at a coarser z resolution (larger dz) which can greatly speed up computation time. The symmetry observed in the amplitude trace can also be exploited to improve the estimate of the in-focus z position.

At this point, I have only mentioned pixel identification based off of amplitude thresholds. The perceptive observer will notice the presence of another trace in figure 2.5. The red trace shown is the normalized phase along the z axis. The observed discontinuity is a direct result of a $1/z'$ relationship between the phase and the reconstruction distance (relative to the in-focus position) for a particular particle[21]. This property is very useful for identifying particles and their in-focus position, but in practice, it is not well behaved enough to use for the initial threshold stage. However, it will be used in later processing stages.

Using the threshold method, a binary mask of the entire reconstructed slice is made marking 'qualified' pixels. To improve the robustness of the analysis method, this mask is then dilated before the pixels are cataloged for further analysis. The next step of the process is to assemble the lists of pixels (now 3D pixels, or voxels) into voxel groups using a connected component labeling technique. In this fashion, clusters of voxels that lie closely to one another in 3D space are identified and merged into groups which ultimately identify them as belonging to the same particle. The output of this analysis for the two particles shown in the example data is shown in figure 2.6b. In this figure, the symbols show the 3D position of all qualified voxels, with voxel group membership indicated by color. The two large particles shown in the example holograms can be seen as the large blue and green groups. The smaller surrounding clusters are either small particles that were not highlighted in the examples, or false positives due to noise.

2.5 Particle Analysis

Once qualified voxels have been grouped into voxel groups, they are processed on an individual basis. The basic approach to this problem is illustrated in figure 2.7. A number of statistics are computed for each (x, y) 'slice' of the voxel group for both amplitude and phase. These include the minimum, maximum, standard deviation and mean of all qualified (as defined by the originally specified threshold) pixels and the standard deviation of the Sobel gradient. These statistics are shown plotted as a function of z in the top and bottom panels on the right hand side of figure 2.7. These traces are chosen due to their tendency to minimize or maximize when the particle is in focus. This provides multiple, independent estimates of the

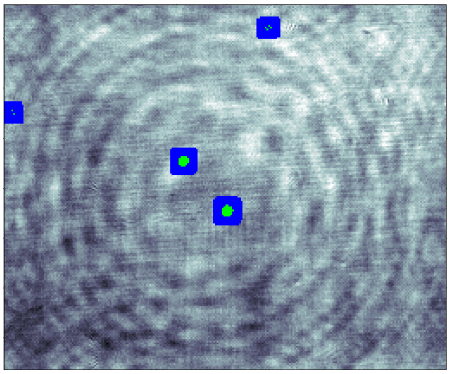

(a) Single reconstructed slice showing qualified pixels

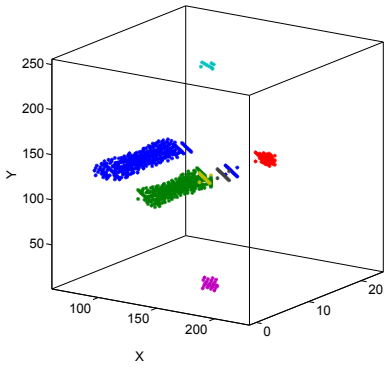

(b) Analyzed voxel groups

Figure 2.6: Reconstructed slice (a) with over threshold pixels (green) and dilated mask (blue) indicated. Pixels identified from multiple slices are grouped using a 3D connected component labeling technique (b). Colors indicate group membership.

in-focus position which is more robust than a single metric. Once the in-focus z location (indicated by a vertical black line overlaid on the traces in figure 2.7) is determined, an area equivalent diameter is computed from the qualified pixels.

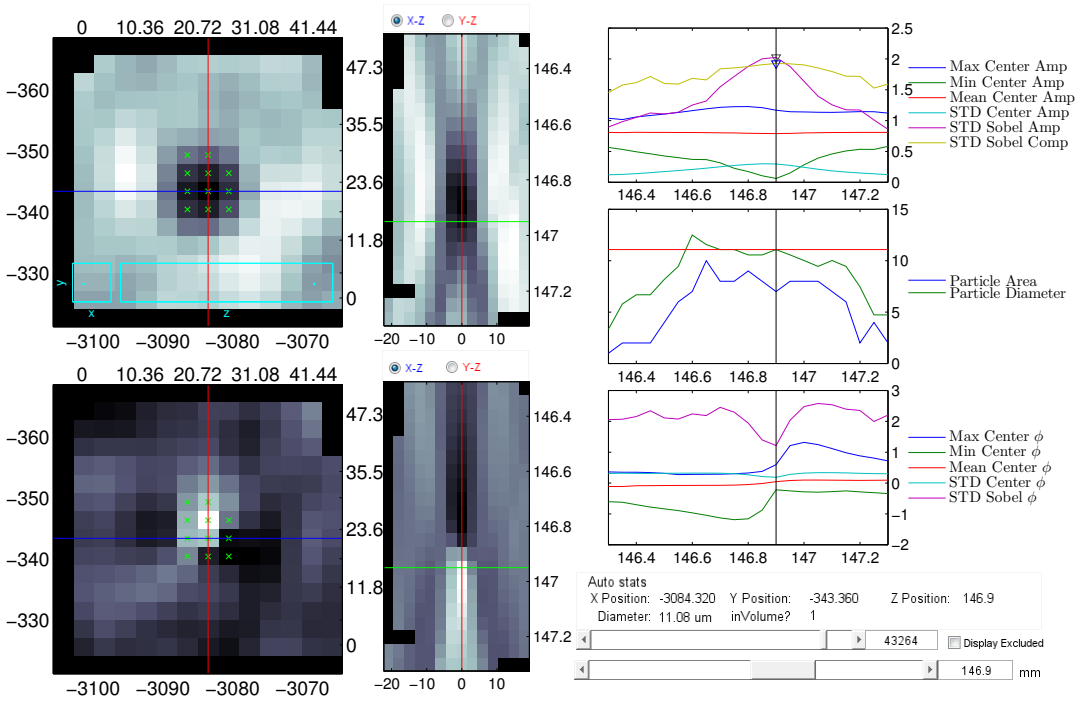

Figure 2.7: Screen shot of particle processing GUI showing a small, spherical droplet. Image panels on left show cross sections of amplitude (top) and phase (bottom) in the (x, y) (left) and (x, z) (right) planes. Colored lines indicate relative location of planes: blue line represents y location of (x, z) plane, and green line indicates z location of (x, y) plane. Statistics (e.g. max/min, mean) from qualified pixels (marked with green 'x's in (x, y) plot) in each (x, y) plane are computed and plotted as a function of z position (right). Peaks and troughs are used as independent measures of the 'in-focus' z position, which is then used to estimate the particle's diameter.

3 Instrument Modifications

The contents of this section are adapted from a final report submitted to the Department of Energy detailing work performed to increase the instrument's technology readiness level[17]. Prior to this work, the instrument was rated at TRL 5, which under the DOE scale corresponds to "Component and/or breadboard validation in relevant environment". It had flown and gathered data under typical operating conditions, but the instrument and data system were merely discrete components and subsystems bundled together in (physically) unified packages. The purpose of this work is to refine and harden the instrument, bringing the readiness level to at least TRL 8 (Actual system completed and qualified through test and demonstration) and making operation possible by a non-specialist.

Through a combination of field and laboratory testing, a number of deficiencies in the existing system were identified and addressed. This involved reworking existing systems (such as the power supply and distribution, and heating subsystems) as well as implementing a new, microcontroller based control system designed to unify and automate control over all instrument subsystems. Design and fabrication of the new control system was performed by Selene Photonics with close collaboration and feedback from myself. This section outlines these changes and the integration of the new control system.

3.1 Description of Original system

The power subsystem in the original design consisted of both 120VAC and 12DC circuits. The instrument is supplied with a 10A, 120VAC connection to the main aircraft power system. It made use of 120VAC to power all heaters as well as the heater control modules. The 12VDC circuit was supplied by a single AC-DC converter which supplied power to the laser, camera, and control system electronics. Power to individual components (120V and 12V) was controlled by a set of power relays. Power distribution and circuit protection was accomplished with a clip-style fuse rack which proved to not tolerate the harsh conditions experienced during flight. This lead to intermittent power issues and at least one damaged component during field trials. In addition, the peak current draw of the laser exceeded the capacity of its relay, causing damage and introducing undesirable behavior.

To combat in-flight temperatures that can fall as low as $-40\,C$, the instrument used cartridge heaters in cold-sensitive area. These areas included the camera and laser head (which both have operating temperatures around $20\,C$) and the instrument tips and optics, where they served to prevent fogging and ice build up. These zones were controlled with independent PID control modules. Cold

chamber testing indicated two potential problems with this layout. The laser control electronics (which are separate from the laser head) were observed to fall out of the standard operating temperature range, and the heater controllers began showing instability at temperatures possible during high altitude flight.

The power relays used to switch power to the laser and camera were part of a larger, serial controlled relay board. Power to individual heaters was also routed through relays on this board to act as an interlock system. This allowed the heaters to be manually disconnected from power if the need arose. The problem with this arrangement was the relays defaulted open on power up and had to be commanded by an operator or logic running on the instrument data system. This requires an operator to run through a startup procedure just to enable basic housekeeping functionality every time the instrument is powered on.

This behavior is not desirable for a number of reasons. Firstly, the instrument must fly on a number of maintenance flights with minimal crew. In this situation, special dispensation is required to ensure that the heaters are properly engaged and programmed. It also requires all safety and sanity checks to be run on a system that is separate from the instrument, introducing multiple points of failure. In field trials, the most commonly observed failures involved the multiple serial connections required to manage the instrument and the instrument data system itself.

Communication between the instrument and the instrument data system was accomplished over three independent serial lines: an RS232 line to the laser controller, an RS485 line to the relay board, and an RS485 line to the heater controllers. This design has a number of disadvantages. The aircraft is only wired to handle a limited number of serial links back to the main cabin that must be shared by all instruments. Consuming an excessive number of lines has the potential to limit the compatibility of the instrument with particular mounting locations, instrument upload configurations and even specific aircraft. In practice, managing multiple serial ports on the data system computer was also problematic and resulted in frequent problems.

Finally, flight testing showed the instrument data system to be a major weak point as well. The system consisted of an external, fire-wire dual hard drive enclosure and a USB serial multiplexer connected to a mac-book pro laptop computer. All components were strapped to a sliding tray which mounted to the aircraft instrumentation racks (shown in figure 3.11a). The external hard drive enclosure holds two 3.5" hard drives configured in a RAID1 configuration. The instrument is capable of recording data at a rate of 3 Gb per minute, necessitating the use of large hard drives to store the recorded data. The RAID1 (mirrored disks)

arrangement helps prevent against data loss from a missed write caused by a sudden acceleration, which is common when flying through convective clouds. These drives are removed at the end of each flight and new, blank drives are mounted in their place for the next flight.

This arrangement works exceptionally well, as it allows for fast offload and reset times and (since two copies of the data exist) provides an enhanced level of data security. The problem discovered in this model is that the drive enclosure chosen for the original system requires the use of proprietary drives, or at least proprietary drive trays (which cannot be purchased separately). This greatly increased the cost to outfit the instrument with enough drives for a full field project. Removing and replacing drives also required tools and access to the rear of the instrument rack, which negated some of the simplicity gained by using a removable drive system.

The frame buffer software used to record the data from the instrument was only available for the windows operating system. This necessitated windows to be installed on apple hardware. This led to severe driver instability which resulted in frequent operating system hangs and crashes. The external network card used to connect the camera to the laptop (through the express slot) also had the tendency to corrupt the driver and and the operating system in the event it was pulled free of the computer while the camera was recording; a situation that was easy to cause by simply pulling the mounting tray out to access the computer. Mitigating this error usually involved performing a full system restore and reinstalling all drivers. Field testing showed that this procedure could not be easily performed in flight. Furthermore, since the instrument can only be controlled by the data system computer, this downtime resulted in a complete loss of control of the instrument.

In addition to the software instabilities in the system, the mounting arrangement of the laptop proved to be problematic. The design of the mac-book pro is such that it draws air through the keyboard to be vented out the back of the case. The mounting arrangement required the computer to be at least partially closed unless the tray was in the extended position. This lead to severe overheating of the computer and required special ducting to be installed from the aircraft's air conditioning unit. The sideways mounting of the computer on the rack also meant that accessing the laptop directly in flight required the operator to contort himself into awkward and unsafe positions. This was not necessary under normal conditions (the computer was accessed remotely through VNC), but was required to recover from the (frequent) crashes.

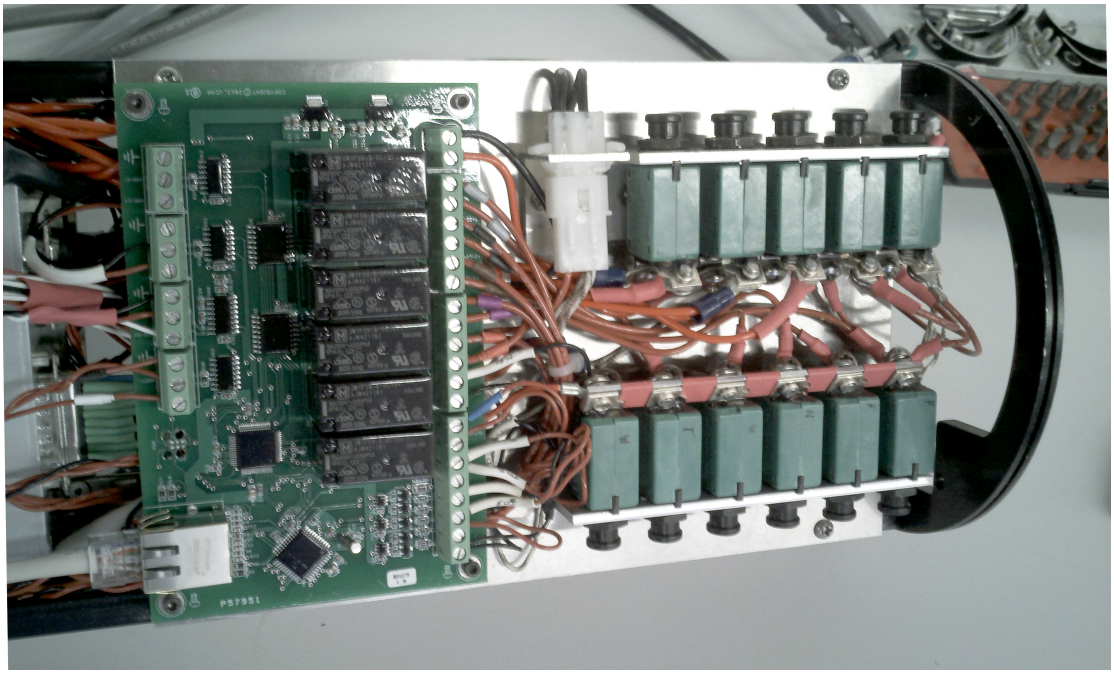

Figure 3.8: Image of new power distribution unit (right) and new control system board (left). White connector (top center) is a connection for a bi-metallic switch responsible for regulating three cartridge heaters embedded in the plate. This is described in section 3.2.

3.2 System Upgrades

To address these issues, the design and implementation of the power supply, heating and communications subsystems on the instrument, as well as the instrument data system were reassessed from the ground up. This consisted of a complete design review including consultation with engineers and technical staff at the National Center for Atmospheric Research to determine the best approach and feature set to implement. My goal with this redesign was to increase the robustness of the instrument while simplifying the requirements to control and manage it.

It was the conclusion of the analysis that substantial changes needed to be made to the power distribution, thermal management and instrument control systems. It was also concluded that the instrument data computer required a complete redesign and replacement. The primary recommendation was to migrate control of the instrument subsystems to an on board, microcontroller based system, allowing for more robust and automated system management as well as unified instrument control. A major element of the redesign was also to implement redundancy and fail-safes in key systems.

Power Systems

The main power system was completely redesigned. The rack of fuses was replaced with two rows of aerospace-grade circuit breakers mounted in custom machined brackets (figure 3.8). This significantly increased the durability of the instrument power system and simplifies diagnostics, as individual subsystems can be more easily isolated. The 12VDC power supply responsible for powering the laser, camera and control system was also replaced with a unit with independent power modules, such that each 12V component is on an isolated supply. The power supply also includes a bus-disable feature that allows each power module to be individually disabled by applying voltage to a control pin. This allows the new control board to disable power to the laser and camera by interfacing directly with the power supply. This removes the requirement of high power relays and also provides smoother power transitions to the components.

Power to individual heater channels is still routed through power relays, which are mounted to and controlled by the new control board. This is a fail-safe measure to ensure that the heaters can only run if the main control board is in a valid state and able to actively monitor and control the heater subsystem.

Thermal Management

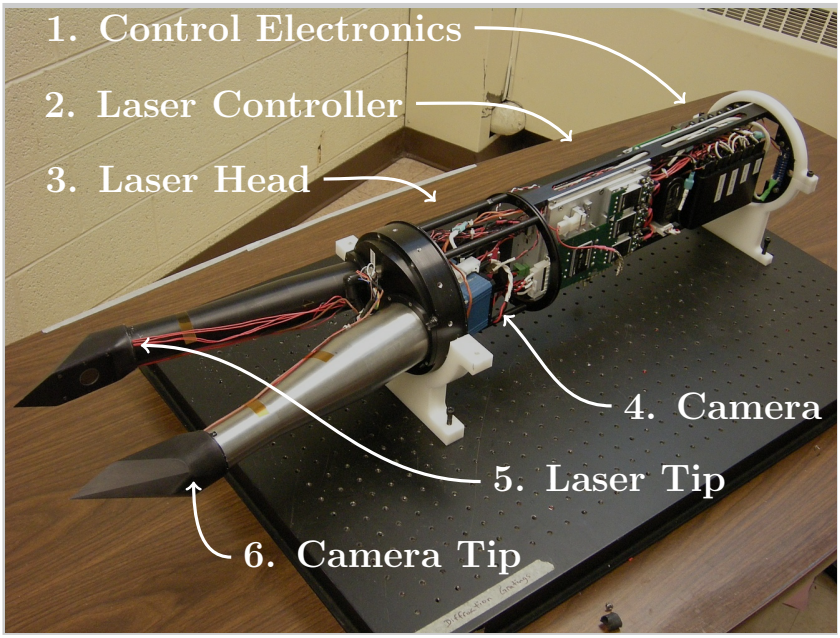

Figure 3.9: Location of six independently controlled heated zones. The heaters for the main control electronics (zone 1) are controlled by a bi-metal thermostat with the remaining zones controlled by 5 independent PID ramp soak controllers. The use of a simple bi-metal thermostat to regulate zone 1 allows the control electronics to be brought back into operating range should the instrument lose power during flight and cool to a temperature that would not allow stable operation of the control electronics.

In order to improve the stability of the control electronics at low temperatures, two additional heated zones are added to the system. These are illustrated in figure 3.9. The two new zones are zones 1 and 2 (control electronics and laser controller). These heaters are embedded into custom designed and machined aluminum mounting plates for the surrounding components.

Adding heaters to the control electronics will only successfully mitigate the low temperature problem if the heaters remain on-line and active throughout the duration of the flight. However, in field trials a failure mode was observed in which the entire instrument lost power for a period of time sufficient for it to cool below the point at which the heater controllers begin acting erratically. In this situation, electronically controlled heaters would not be able to recover and bring the thermal state of the instrument back under control. To remedy this situation, the 'control electronics' zone makes use of a simple bi-metal thermostat calibrated for 5 °C. In the event of a cold start, this will bring the control electronics back to operating temperature, at which point they can resume operation.

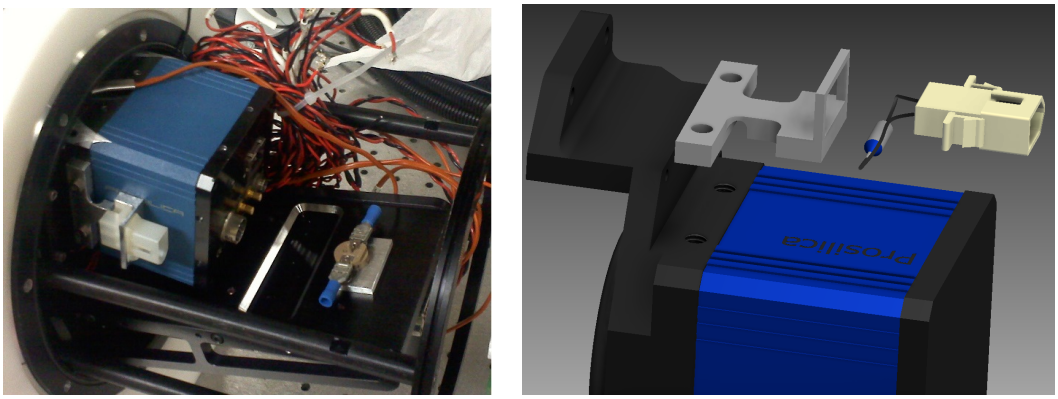

(a) Photograph of thermal fuse mounting (left) on camera and thermal breaker on laser head mounting plate

(b) Exploded view of camera thermal fuse and mounting arrangement.

Figure 3.10: Depiction of thermal fuse mounting arrangement on camera and laser head mounting plate. Thermal fuses and breakers are installed in series with the main power to the cartridge heaters to serve as fail-safe protection against a runaway heater.

The case of a cold start also introduces the possibility of damage to components due to excessively fast heating. To address this situation, all control over the heaters is moved to the new control board. Independent PID heater control modules are still used to control the five actively regulated zones. The new control system communicates with and commands these modules over an RS485 serial bus. On startup, the new control system initializes communication with the temperature controllers to verify their state. Once verified, the control system resets the set point on all controllers to $-40\,^{\circ}\mathrm{C}$, closes the relays and enters into active temperature control mode.

In active temperature control mode, the control system is programmed to implement sliding mode control. Every ten seconds, the control system polls the heater control modules to read the current temperature of their respective components. If the difference between this temperature and the desired operating point (OP) is greater than $5\,^{\circ}\mathrm{C}$, the set point on the controller is reset to be the current measured temperature plus $5\,^{\circ}\mathrm{C}$ (or $T - 5\,^{\circ}\mathrm{C}$ if $T > OP$). Once the temperature reaches $\pm 5\,^{\circ}\mathrm{C}$ of the desired operating temperature, the set point is set to the operating temperature.

In addition to programmatic temperature control, non-resettable thermal fuses are installed in the heated components (figure 3.10). These fuses are designed to interrupt the heater power circuit in the event they exceed a set temperature. These are added to protect against extreme over-temp conditions if equipment were to fail and cause a heater to become permanently engaged.

Communication Subsystem

In addition to automated control over the heater control modules, the new control system also greatly simplifies communications between the instrument and the user/data system. The three serial connections have been replaced by a single, redundant connection. The primary connection to the instrument is now over a single RS485 line that runs directly from the instrument (through wing wiring) to the instrument data system.

Interaction with the instrument over the serial line is handled through a custom command line interface (CLI). The CLI syntax is designed to be machine friendly (allowing for easy integration with other software tools, such as LabVIEW) while still being human readable. This interface allows complete control over the instrument and its subsystems, including manual control over the interlock relays, control over the power supply bus-disable, and adjustment of heater operating temperatures. This CLI is augmented with a custom LabVIEW based user interface installed on the instrument data system.

In addition to serial communication, the laser controller also has a series of digital output channels to indicate laser status, such as if the laser head is warmed up and "ready" for emission, if the laser is actively emitting and if the laser is in an error state. These channels are read by the control board and are made available through the CLI. Direct communication with the laser (to start/stop lasing, read error and status codes, etc) is handled by relaying commands in the laser controller's native syntax through the main control board using a command prefix. This allows for native control over the laser without requiring a separate connection. It also allows for the main controller's on-board logic to interface with and control the laser, although this feature is not currently implemented in the firmware.

The control system is also equipped with a 10/100 Ethernet port designed to patch into the aircraft's data network. This network connection provides redundant telnet access to the instrument from any workstation in the aircraft and allows the control system to broadcast a $1\,Hz$ housekeeping data stream (consisting of temperature readings) to the main aircraft data-logger. This redundancy in communication ensures that the instrument can be easily monitored and controlled even if the instrument data system completely fails. The data broadcast also ensures that a history of the instrument's thermal condition is automatically maintained in the flight records regardless of the status of the instrument data system.

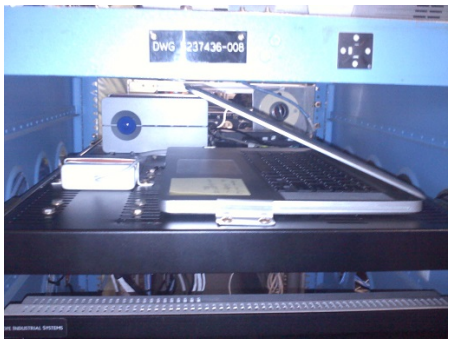

(a) Old instrument data system comprised of laptop computer (right), external hard drive (left) and serial multiplexer (underneath - not shown).

(b) New instrument data system. Entire system is housed in a single 3U server chassis. New system includes redundant system drives and front opening enclosures for data drives to simplify data offload.

Figure 3.11: Comparison of old instrument data system (a) to new system (b). All components have been integrated into a single system, reducing complexity and increasing robustness.

Instrument Data System

In order to address the concerns with the original instrument data system, the laptop computer was replaced with a 3U rack mount server (shown in figure 3.11b). The form factor of the 3U server occupies the same amount of space (if not less) as the original system, while greatly simplifying and consolidating cable routing and external connections. Also, since the new system is designed to be rack mounted, the cooling system is more than sufficient to keep system temperatures stable under all observed flight conditions without additional external cooling.

The original concept of using two 3.5" hard drives in a RAID1 configuration for recording the data is preserved. The external enclosure is replaced by a pair of front access drive bays designed to accept bare 3.5" SATA drives. The ability to accept bare drives removes the requirement of purchasing and mounting special drive trays. This reduces the overall cost of the system while simultaneously reducing complexity and possible points of failure. The procedure to swap drives with the new drive bays is also significantly simpler, reducing offload/upload time.

A major increase in system stability was achieved simply by no longer running Windows on Apple hardware and having all peripheral components firmly mounted within the computer chassis. To further increase the reliability of the system, a solid state drive is used for the main system disk, with a second, offline, mirror installed in another front access drive. The second drive provides a fail-safe backup that can be used to reboot the system should the main system disk become corrupted in flight. Mounting the system drives in front access bays also allows all system disks to be removed for replacement or re-imaging without removing the

computer from the rack.

3.3 Instrument Testing

The new instrument configuration and data system were tested as part of the Instrument Development and Education in Airborne Science (IDEAS) campaign in November of 2012. The testing involved six flights on the University of Wyoming King Air (figure 2.1a) sampling convective clouds over south-central and south-eastern Wyoming.

The instrument performed as intended throughout flight testing with only two minor concerns. It was observed that static charge build up on the aircraft and instrument can possibly lead to random resets of the instrument control system. It is believed that this is related to charge accumulation on the large, nylon flow shroud on the front of the instrument. Attempts to bleed excess charge from the shroud did not improve the condition. It is not clear at this time if this sensitivity is a feature of the new design or the specific mounting and connection arrangement used with the aircraft. This question will be addressed in further testing in the fall of 2013.

It was also observed that the new power supply produces more heat than expected, causing potential overheating problems with the laser controller electronics if run for extended times on the tarmac. Once in flight, airflow over the canister exterior is sufficient to sink the excess heat. This problem is currently being addressed by keeping the laser and camera power modules disabled while on the ground, except for short periods needed to test the instrument prior to flight. No long term solution is planned at this time.

Even with the observed glitches with the new design, the instrument and data system showed vast improvements in stability and functionality and the ability to be run by a non-specialist in the field. This is justification for declaring the instrument upgraded to TRL 8 with the potential to be upgraded to TRL 9 after trials in the fall of 2013.

4 Holosuite - Reconstruction Software

The ultimate goal of the project was to make the entire process of hologram recording and processing more simple and robust. The improvements to the instrument and data system greatly improved recording and measurement but did not address the ability to process holograms into meaningful scientific results. This next task involves improving the code that is used to perform the reconstruction and analysis procedure outlined in section 2.3.

The basic code and methods used to reconstruct and analyze particles from holograms was previously developed by Fugal[6]. This code was in the form of a series of matlab scripts that were not well generalized and required specialized knowledge to modify properly to adapt to a particular reconstruction problem. To make the new code simple to use without losing flexibility or power, it was decided to divide the problem of reconstruction and particle processing into a series of classes. These classes are written in object-oriented matlab and serve as a low level framework upon which higher level scripts and functions are built.

The section that follows contains a description of these classes and their main functionality. Also described will be select tools and graphic interfaces built on top of this framework which simplify configuring and interacting with the reconstruction process. They are designed to be simple enough that a non-specialist can use them to successfully process and analyze hologram data. This code was written in close collaboration with Dr Fugal at the Max Plank Institute für Chemie.

4.1 Main Framework

The main framework consists of four main classes: config, img, propagator, and particle. Each class is written such that it can perform its specific function as a stand alone object, or be linked to a large scale process through the 'config' object. The 'config', 'img' and 'Propagator' classes also all inherit the 'handle' parent class and make use of event driven programming. This means they throw notifications when key parameters are changed and key methods are called. In object oriented matlab, a copy of a handle class object is actually a pointer to the original. This pass-by-reference and event driven behavior allows the existing set of graphical tools to be easily extended without modifying their core code.

Config

As the name suggests, the 'config' class is designed primarily to handle the storage of configuration data for use in the hologram reconstruction process. In

order to enable efficient batch processing of holograms and maintain a record of which settings were used to reconstruct a set of holograms, it was decided that text based configuration files should be implemented. At the basic level, the 'config' class handles the translation between the file-based configuration data and a structure in memory that can be interacted within matlab code.

In addition to reading and writing configuration settings, the 'config' class is also designed to simplify the process of finding files and manipulating file names. For instance, one parameter consists of a regular expression string that defines a 'hologram file' (that is, a file name must match the regex to be considered a hologram). This greatly simplifies the process of loading hologram data, as the user can just request (through a method) a list of all holograms instead of manually filtering the file list. The 'config' class also allows for the definition of sequences, which are defined as "$< starting\,file\,name >:< stride >:< ending\,file\,name >, < sequencename >$". These sequence definitions make it simple to subdivide a large directory of holograms into smaller pieces and can be used to direct automated reconstruction processes.

One of the most important aspects of the 'config' class is that it inherits the handle class. By using a config object in the remaining classes in the framework to store primary configuration parameters, configuration settings are updated in all objects immediately. The main driving force with this style of architecture is to ensure all objects are working with the same set of parameters, and if one parameter is changed anywhere, then that change is reflected immediately in all objects.

Img

The 'img' class is designed to simplify reading, processing and formatting image data; either to prepare a hologram to be reconstructed or to post-process the reconstructed slice. It can accept either raw image data or a path to an image file which it will load and format to the proper data type. The class is designed for two main purposes: image filtering and pixel segmentation through the application of thresholds.

The 'img' class provides a flexible and dynamic method to filter the full complex image as well as the amplitude and phase components separately. Each filter is specified as a function handle and parameter structure (which is passed to the filter function along with the image to be filtered at run time). Values in the structure can also reference parameters and methods of the 'config' object (if one is assigned) through the use of macros. This extends the 'global' reach of the 'config' class into user supplied functions and helps maintain a high level of consistency

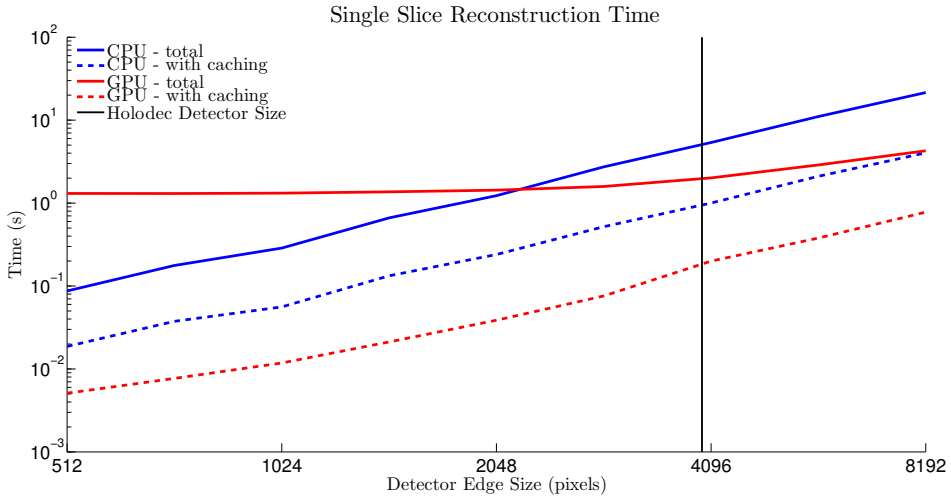

Figure 4.12: Single slice reconstruction times computed using 'Propagator' object comparing performance of CPU and GPU processing. Solid lines indicate time to reconstruct a single slice from beginning to end, while dashed lines indicate the time to reconstruct a slice with caching enabled. For a reconstruction process, the first slice would take the total (solid line) time with each additional slice costing the cached time (dashed line). Under some circumstances, the overhead required to initialize the GPU makes processing on the CPU faster, however this is completely mitigated by the caching process. For Holodec size holograms (vertical black line), the GPU with caching enabled results in almost a full order of magnitude improvement over CPU processing with pre-caching and two full orders over direct reconstruction on the CPU.

and repeatability. The class also (optionally) maintains an automatically updated cache of filtered images. This feature helps to minimize redundant processing, keeping processing times as short as possible.

The process of identifying pixels based on amplitude (and optionally phase) thresholds is also handled through the 'img' class. This enables a user to create an 'img' object, load configuration data (containing relevant thresholds and other settings) and processes hologram slices into lists of pixels with only a few commands.

Propagator

The 'Propagator' class houses all of the methods responsible for performing the numeric hologram propagation. Of all the classes, the 'Propagator' class functions at the lowest level and exports the smallest feature set. For a given hologram, a full reconstruction can involve computing several thousand slices. This puts extreme weight on the efficiency of the 'single slice' reconstruction time.

The reconstruction process (discussed in section 2.3 and in more detail in Fugal *et al*[7]) is seen to consist of two Fourier transforms and an element-wise multiplication by a complex exponential. Both of these operations can be considerably accelerated (especially for large images) through the use of graphic processing units (GPUs). While matlab does offer a simplified interface to working with data on GPUs, it is not as transparent as desired. To simplify this problem, the 'Propagator' class is designed to form a wrapper around the reconstruction process that allows the user to switch between using CPU based processing and GPU based processing on the fly and completely transparently. The class also implements sanity checking and error handling to attempt to handle errors encountered during processing on the GPU, dynamically transitioning over to CPU based processing if needed.

In addition to reconstructing on GPUs, an additional speedup can be recognized by introducing a caching system. In the angular spectrum propagation method, the initial transform of the hologram field as well as part of the propagation kernel (and the low pas filter) do not vary with the reconstruction distance. Therefore these portions of the process can be computed once for a given hologram and cached. The impact of the caching scheme and GPU processing is shown in figure 4.12. This benchmark was generated with an Intel hexcore E5645 processor at 2.6GHz and a graphics card with an NVIDIA GTX TITAN GPU with 2688 cores running at 837 MHz. Solid lines indicate the total amount of time required to reconstruct a single image slice including all steps of the process This also includes the time to initialize the GPU and transfer data into GPU memory. This overhead actually makes processing on the CPU faster for images smaller than 2048×2048. However, when this overhead is removed by implementing the cache, the GPU is consistently faster by nearly a full order of magnitude. This results in a speed increase from 1s per slice on a CPU to 0.1s per slice on the GPU for Holodec size holograms. For a single hologram reconstruction of 3000 slices and a frame rate of 3Hz, this allows for a data processing rate of 15 minutes per second of recorded data compared to 2.5 hours per second using CPU based processing.

Particle

Once the hologram has been reconstructed, and the qualified pixels cataloged and reassembled into voxel groups (see section 2.4 for details), the groups need to be further analyzed to extract information about the particle This information includes the particle size and a more accurate position of the particle center within the sub-volume. The process of extracting these parameters amounts to searching a three dimensional, complex valued field for recognizable patters (e.g. figure 2.5). This exact process is still the focus of continuing work and represents the 'bleeding edge' of the field.

Because there is still so much development occurring in this area, the original intent of the 'particle' class was to simply ease the process of interacting with the voxel groups to speed the development of these algorithms. The data for each voxel group is stored as a list of pixel indices and values which need to be reassembled into a three dimensional block for analysis. This class performs this task, as well the mapping between the local sub-volume coordinate system and the global hologram coordinate system.

In addition to simply manipulating the voxel data, the 'particle' class also incorporates a construct that is used to determine particle position and size. It divides the pattern recognition process into a series of stages of decreasing dimensionality. The first stage is to apply a function to the three dimensional complex valued data to enhance the pattern of interest. Functions typically used are amplitude, phase, sobel gradient (of amplitude and phase), and amplitude and phase with a threshold mask applied to remove 'non-qualified' voxels. These 'blocks' can then be paired with functions that reduce them to two dimensional 'traces'. These 'traces', can then be reduced in the same fashion to a single 'value'.

In this fashion, a three dimensional, complex valued array can be manipulated into a single representative value. The hope is to eventually derive a set of metrics that can be used to form a point-cloud, with regions of state space corresponding to particle validity, phase (ice vs liquid) and possibly higher order features such as crystal habit. This full implementation has not been realized quite yet, but the method is currently used in the particle analysis method discussed in section 2.5. In this situation, the 'traces' are profiles along the z axis that are chosen to maximize (or minimize) close to the position in which the particle is in focus. The functions generating 'values' return the point along the z axis where the minimum/maximum occurs. These represent independent measurements for the in-focus position, which can then be averaged together to obtain the best estimate.

As a single hologram can contain upwards of 1000 particles, the 'particle' class has been extended to a 'particleGroup' class which adds methods to processes particles in bulk. Part of this is the addition of a threshold based particle qualification algorithm which is used to determine if the voxel group is an actual particle or simply a false alarm. This classification is based on whether or not the group passes a series of user-defined criteria, such as minimum z-depth, maximum/minimum phase and maximum/minimum amplitude. This allows an entire hologram's worth of particles to be loaded, filtered and analyzed with minimal keystrokes.

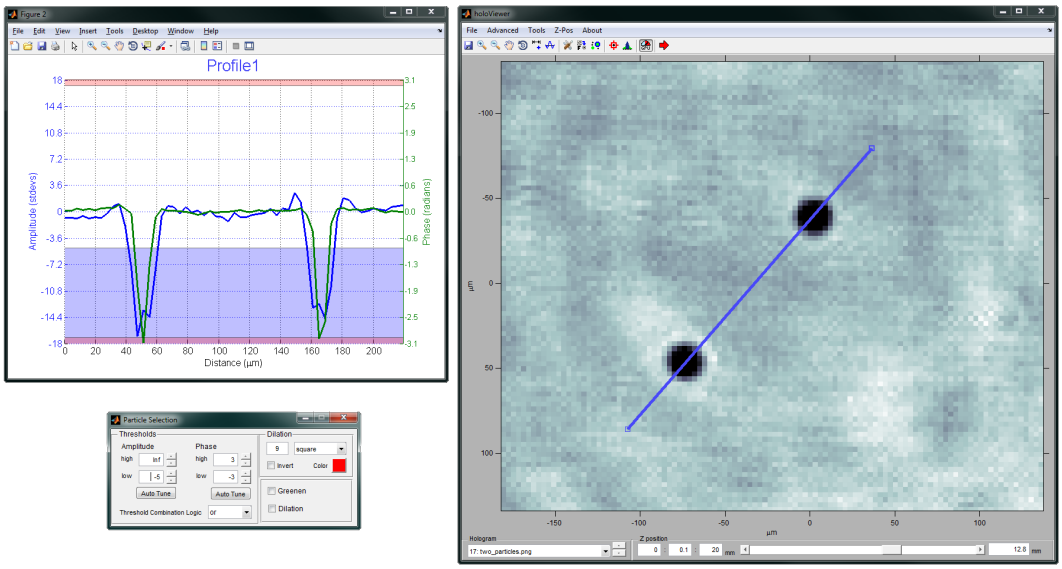

Figure 4.13: Holoviewer main panel (right) showing two particles in focus with a profile indicator (blue line). Profile panel (left) shows amplitude and phase values across the indicated line with shaded patches indicating current thresholds. Particle Selection panel (bottom left) illustrates typical panel used to allow users to update settings.

4.2 Supporting Tools

While the tools discussed in the previous section are designed to greatly simplify the creation of custom reconstruction and analysis scripts, a set of tools have already been developed around them. These tools are designed to perform bulk hologram reconstruction as well as allow *ad hoc* analysis of individual holograms and voxel groups. Since the framework and code is common between the two processes, the graphic user tools can be used to setup and review the batch process with a high confidence that what the user visually sees is what the automated process 'sees'.

Holoviewer

Holoviewer (shown in figure 4.13) is a graphic front end that allows for on demand reconstruction of individual slices. The reconstruction process used exactly mirrors the process used in the production code. The exact filters used and their parameters are not hard coded, but are rather managed dynamically through the use of 'img' objects. This allows a user to adjust filters and filter parameters and visualize their effect on the reconstructed field immediately.

In addition to manipulating filters, holoviewer also provides a number of tools to aid in the threshold selection process. A threshold selection tool panel is provided

by default that allows a user to adjust the threshold and dilation parameters dynamically. The effects of these thresholds can be overlaid onto the reconstructed slice, highlighting the pixels that would be qualified by the current threshold and dilation settings. This display is updated in real-time, allowing a user to quickly gauge the effects of the threshold settings on particle selection and noise rejection.

Besides simply highlighting pixels qualified by the thresholds, additional tools are included to help diagnose threshold settings and the reconstruction in general. One such tool is the hologram profile tool which allows a user to generate a profile view of a region of a hologram. The two dimensional version of this profile tool is illustrated in figure 4.13, showing amplitude and phase profiles along the blue line, with threshold values illustrated by color shaded regions.

All settings are managed through the use of a 'config' object, allowing them to be read from and written to a text based file which can be shared with the batch reconstruction process. This allows holoviewer to not only serve as a configuration tool to select proper settings for a set of holograms, but also to review holograms using the same settings to diagnose problems encountered with the reconstruction process.

SeePartBlock

SeePartBlock is a tool used to hand analyze and visualize voxel groups by providing a graphic front end to the 'particle' and 'particleGroup' classes. The main GUI window is shown in figure 2.7, illustrating the analysis of an ($11\mu m$) cloud droplet. The panels on the left are designed to show the amplitude (top) and phase (bottom) portraits of the voxel group along the (x, y) plane (left) and $(x, z)/(y, z)$ planes (right - (x, z) shown). The position of the cross sectional planes can be moved, allowing for the user to visualize and explore the full three dimensional extent of the voxel group

The plots shown on the right illustrate select traces along the z dimension used to determine particle focus position (discussed in section 4.1). These traces can be dynamically updated through direct interaction with the parent 'particleGroup' object. They allow for the efficacy of the selected traces to be gauged on a visual basis, which was instrumental in formulating the existing set used as well as determining proper thresholds for particle qualification.

4.3 Bulk Reconstruction Scripts

To simplify the problem of reconstructing holograms en masse, a set of scripts have been developed and included with holosuite. These scripts are designed to handle each step of the reconstruction processes in an automated fashion and include features such as advanced error handling and parallelization. These scripts divide the process into three main parts: reconstruction of the hologram into slices. assembling the slices into voxel groups, and analysis of the voxel groups into particle statistics.

Each of these three stages represents natural breaks in the processing flow. Each set of holograms is processed through a single stage before moving to the next with the results cached to disk. As the processing scheme (and therefore parallelization strategy) between stages is vastly different, this processing scheme greatly reduces the amount of time spent reconfiguring the workers. The producer-consumer style processing also enables the process to be easily divided up amongst multiple machines. This allows for specialization of machines, which has the potential to lower the cost of implementation on larger scales.

5 Concluding Remarks

In this manuscript, I describe work I have performed with the Holodec instrument to advance its technology readiness level from TRL 5 to TRL 8. Through collaborative and independent efforts, I have redesigned the instrument and data system to increase reliability, functionality and versatility. Field trials in the fall of 2012 showed the upgrades to be successful with only a few minor potential issues to improve upon. The net result of this work is to transform an instrument that was in a 'flying breadboard' (TRL 5) state into a single, unified system, capable of flying on an increased range of platforms and operated by a non-specialist (TRL 8).

In addition to improving the instrument hardware, I also made a significant contribution towards improving the software used to process digital holograms. By introducing a new object oriented based framework, I was able to abstract the complexities of the reconstruction process to create a set of powerful, yet simple to use tools. This framework is used to build a set of graphic interfaces and bulk reconstruction scripts that allow a user with limited experience in the field to successfully explore and reconstruct holographic data.

[1] DOE G 413.3-4A, Technology Readiness Assessment Guide. `https://www.directives.doe.gov/directives/0413.3-EGuide-04a/viewcc`. Accesed: 2012-9-21.

[2] P. R. A. Brown. Use of holography for airborne cloud physics measurements. *joat*, 6:293–306, 1989.

[3] P. R. Field, R. Wood, P. R. A. Brown, P. H. Kaye, E. Hirst, R. Greenaway, and J. A. Smith. Ice particle interarrival times measured with a fast fssp. *J. Atmos. Oceanic Techl.*, 20:249–261, 2003.

[4] J. Fugal and R. Shaw. Cloud particle size distributions measured with an airborne digital in-line holographic instrument. *Atm. Meas. Tech.*, 2:259–271, 2009.

[5] J. Fugal, R. Shaw, E. Saw, and A. Sergeyev. Airborne digital holographic system for cloud particle measurements. *Appl. Optics*, 43:5987–5995, 2004.

[6] J. P. Fugal. *in-situ Measurement and Characterization of Cloud Particles Using Digital in-line Holography*. PhD thesis, Michigan Technological University, 2007.

[7] J. P. Fugal, T. J. Schulz, and R. A. Shaw. Practical methods for automated reconstruction and characterization of particles in digital in-line holograms. *Meas. Sci. and Tech.*, 20, 2009.

[8] J. Goodman. *Introduction to Fourier Optics*. McGraw Hill, 2 edition edition, 1996.

[9] A. Korolev. Probe tips for airborne instruments used to measure cloud microphysical parameters, Jan. 4 2011. US Patent 7,861,584.

[10] A. Korolev and G. Isaac. Shattering during sampling by oaps and hvps. part i: Snow particles. *J. of Atmos. and Oceanic Tech.*, 22:528–542, 2005.

[11] A. Korolev, G. Isaac, S. Cober, J. Strapp, and J. Hallett. Microphysical characterization of mixed-phase clouds. *Q. J. R. Meteorol. Soc.*, 129:39–65, 2003.

[12] A. V. Korolev, E. F. Emery, J. W. Strapp, S. G. Cober, G. A. Isaac, M. Wasey, and D. Marcotte. Small ice particles in tropospheric clouds: fact or artifact? airborne icing instrumentation evaluation experiment. *Bull. Amer. Meteor. Soc.*, 92:967–973, 2011.

[13] K.-N. Liou. Influence of cirrus clouds on weather and climate processes: A global perspective. *Monthly Weather Review*, 114:1167–1199, 1986.

[14] G. G. Mace, Y. Zhang, S. Platnick, M. D. King, P. Minnis, and P. Yang. Evaluation of cirrus cloud properties derived from modis data using cloud properties derived from ground-based observations collected at the arm sgp site. *J. Appl. Meteor.*, 44:221–240, 2005.

[15] S. Oshchepkov and H. Isaka. Inverse scattering problem for mixed-phase and ice clouds. part i: Numerical simulation of particle sizing from phase-function measurements. *Appl. Opt.*, 36:8765–8774, 1998.

[16] J. L. Schols, J. A. Weinman, G. D. Alexander, R. E. Stewart, L. J. Angus, and A. C. L. Lee. Microwave properties of frozen precipitation around a North Atlantic cyclone. *J. Appl. Meteorol*, 38:29–43, 1999.

[17] R. Shaw, S. Spuler, M. Beals, N. Black, J. Fugal, and J. Lu. Final report on holodec 2 technology readiness level. Technical report, DOE Office of Science Atmospheric Radiation Measurement (ARM) Program (United States), 2012.

[18] S. Spuler and J. Fugal. Design of a digital, in-line, holographic imaging system for airborne measurement of clouds. *App. Optics*, 50:1405–1412, 2011.

[19] G. Stephens, S. Tsay, P. Stackhouse Jr, and P. Flatau. The relevance of the microphysical and radiative properties of cirrus clouds to climate and climatic feedback. *J. Atm. Sci.*, 47:1742–1753, 1990.

[20] P. Webster. The role of hydrological processes in ocean-atmosphere interactions. *Rev. Geo.*, 32:427–476, 1994.

[21] W. A. Yang, B. Kostinski, and R. A. Shaw. Phase signature for particle detection with digital in-line holography. *Optics Letters*, 31:1399–1401, 2006.